

Article

Visualization of Patterned Modified Surfaces in Condensation and Frosting States

Kai-Shing Yang *, Wei Lu and Yu-Lieh Wu

Department of Refrigeration, Air Conditioning and Energy Engineering, National Chin-Yi University of Technology, Taichung 411, Taiwan; tonylui6666@gmail.com (W.L.); wuy1@ncut.edu.tw (Y.-L.W.)

* Correspondence: ksyang@ncut.edu.tw; Tel.: +886-4-2392-4505 (ext. 8231)

Received: 11 November 2019; Accepted: 22 November 2019; Published: 23 November 2019



Abstract: In this study, a novel, thorn-shaped, containing, hydrophilic, and hydrophobic surface is proposed to have a better condensate drainage characteristic and to delay the required time for frosting. By using a hydrophilic and hydrophobic mixed thorn-shaped surface created by screen printing, the design makes use of the differences in the wettability gradient to achieve rapid condensate drainage and to lengthen the time for frosting. The results of a frosting experiment indicated that the droplet adsorption and combination and discharge effect in the thorn sample were substantial. The drainage effect increased the surface renewal rate and inhibited ice layer growth on the thorn sample by 52.4% compared with that on pure copper surface. The heat transfer coefficient of the thorn sample during frosting was approximately 16.2% higher than that of pure copper surface. In addition, the defrosting results indicated that the defrosting time of the thorn sample was almost equal to that of the pure copper sample. However, large droplets were easily stagnated at the structural junction due to contact angle hysteresis after defrosting.

Keywords: surface modification; wettability; condensation; frost

1. Introduction

Heat exchangers have been widely used in modern industrial and mechanical equipment and play a key role in processing and manufacturing. Due to concerns regarding environmental pollution and energy utilization, improving the energy efficiency, particularly the fin frosting phenomenon of finned tube heat exchangers used in air conditioning and refrigeration systems, has become a crucial issue. In addition to reducing system efficiency, accumulation of a frost layer causes an increase in the air-side pressure drop and fan power consumption [1]. Moreover, melted frost water can reduce heat transfer and cause refrosting, which reduces energy efficiency appreciably. To solve the aforementioned problems, many scholars have studied defrosting technology for heat exchangers. The defrosting-related technologies can be classified into active and passive designs [2]. Active designs increase the defrosting capacity through the energy input method. Many researchers utilized electrohydrodynamic (EHD) technique to reduce the frost amount [3]. Although active designs can considerably improve the defrosting capacity, they also increase system complexity and consume additional energy.

Passive defrosting designs are mostly adopted through surface treatment such that no additional power is input into the system, and no additional components are required. Passive defrosting designs are a recent study trend. Liu et al. [4] developed a frost resistance coating, and their results revealed that applying the coating on metal surfaces can delay the initial frost crystal formation time by at least 15 min. The frost layer thickness was also reduced by 40%. When relative humidity (RH) of the environment was less than 60%, and the temperature of the flat surface was higher than $-10\text{ }^{\circ}\text{C}$, the coated surface could remain unfrosted for 3 h. By contrast, the uncoated copper surface was completely

covered by a thick frost layer. The results of Liu et al. indicated that passive designs can be effectively created through a simple structural design and frost layer delaying process.

The frost formation stage is mainly divided into condensation, dropwise freezing, ice crystal formation, and growth process, whereas the condensation phenomenon can be further divided into filmwise condensation and dropwise condensation depending on the surface characteristics. The surface characteristics are mainly based on the size of the contact angle, which acts as a wettability indicator for a material surface. The contact angle is measured by surface tension of static equilibrium of solid, liquid, and gas. Young [5] first introduced a calculation theory (i.e., Young's equation) in 1805, where a surface with a contact angle of less than 90° is defined as hydrophilic and with a contact angle higher than 90° is defined as hydrophobic. The surface energy decreases when the surface is hydrophilic. Water is more likely to wet a hydrophilic surface, and filmwise condensation easily occurs on a hydrophilic surface. The surface energy increases when the surface is hydrophobic. On a hydrophobic surface, molecules and water repel each other and dropwise condensation is likely to occur. However, for both hydrophobic and hydrophilic surfaces, the temperature gradient of the inner condensate forms a heat resistance for reducing the heat transfer capability between the surface and air.

Some scholars have used surface modification methods to study different properties of the condensation phenomenon and have explored the derived heat transfer effectiveness and surface phenomena. Vemuri and Kim [6] used 1-octadecanethiol to grow a self-assembled monolayer on a copper alloy surface for achieving dropwise condensation, and the resulting heat transfer rate was three times higher than that in bare copper alloy. The heat transfer rate was increased by approximately eight times when operating under atmospheric pressure, and a theoretical formula for predicting the size distribution of the condensed droplets was derived. Ma et al. [7] conducted experiments regarding the non-condensable gas concentration, saturation pressure, and surface undercooling on vertical plates. The findings indicated that the heat transfer coefficient (HTC) of dropwise condensation was 30% to 80% higher than that of filmwise condensation even if the concentration of non-condensable gas was increased to appreciably deteriorate the HTC. This is because the combination and slippage of droplets led to a rapid surface renewal rate, which increased the surface heat transfer area, thereby offsetting the negative influence of non-condensable gas. Furthermore, although the liquid film was eliminated, some condensate remained due to the large surface wettability. Thus, the condensate added thermal resistance could not be completely eliminated.

Several researchers have designed mixed hydrophilic and hydrophobic surface patterns to enhance surface droplet movement and slippage. Chatterjee [8] used Teflon coating to develop a circular island and tree shapes composed of 25% hydrophilic and 75% hydrophobic area with a fixed velocity of vapor. The results indicated that the heat transfer coefficient of the mixed surface was approximately 7.5% higher than that of a completely hydrophobic surface. In addition to being influenced by gravity, the droplet departure diameter and frequency were influenced by the diameter of the hydrophilic islands in the island pattern. Small islands were more likely to cluster, thereby reducing the time taken for droplets to reach the maximum droplet radius, increasing the droplets' departure frequency, enhancing surface renewal, and increasing the surface heat transfer coefficient.

Peng et al. [9] designed an alternating hydrophilic and hydrophobic pattern and found that the heat transfer coefficient increased as the width of the hydrophilic area increased. This result was obtained because a reduction in the liquid film thickness can decrease the thermal resistance. Moreover, the heat transfer coefficient increased with a decrease in the width of the hydrophobic area. Because the maximum droplet radius decreased as the width of the hydrophobic area decreased, the distribution density increased. The hydrophobic area enhanced its heat transfer capability with small droplets during dropwise condensation. In the experiment, the optimal widths of the hydrophobic and hydrophilic areas on the mixed surface were 0.55 and 0.45 mm, respectively. Therefore, by using an appropriately designed mixed surface, the heat transfer of dropwise condensation can be adjusted and enhanced. Alwazzan et al. [10,11] designed a linear pattern composed of a hydrophobic (β) area and high wettability (α) area. The droplets in the β area were combined to utilize the wettability

gradient between both areas to drive the droplets from the β area to the α area. Finally, the α area acted as a drainage path to remove surface-condensed water for increasing the removal rate. The heat transfer coefficient was increased by 4.8 and 1.8 times compared with that for filmwise condensation and dropwise condensation, respectively.

Yang et al. [12] designed an interlaced pattern of parallel oblique angles to compare hydrophilic, superhydrophilic, and hydrophobic surfaces. They claimed that the maximum average Feret diameter of the droplets on a mixed surface was approximately 80% to 90% smaller than that on the hydrophobic surface. The heat transfer coefficient of the mixed surface was approximately 3% to 9% higher than that of the hydrophobic surface due to the movement and discharge mechanism. Moreover, the heat transfer coefficient of the mixed surface was approximately 6% to 16% higher than that of the hydrophilic surface. Yang et al. [13] proposed an improved star design that can effectively enhance the heat transfer performance by 15.3% to 30.4%. Alheshibri et al. [14] discovered that when a droplet was at the tip of the hydrophilic surface, it slowly moved toward the divergence. The larger the angle of divergence, the faster the droplet moved, and the surface tension produced by the structure became higher than the gravity at a certain angle. Mahapatra et al. [15] placed a superhydrophilic surface track in the center of a hydrophilic pattern and staggered parallel to the hydrophilic pattern. The heat transfer coefficient of the design at 29.9% filmwise area increased by 34.4% compared with that for completely dropwise condensation.

The aforementioned studies have explained the condensation heat transfer enhancement benefits of surface modification, and surface modification technology has been used in frosting studies. Liu et al. [16] investigated the effect of condensation on a superhydrophobic modified surface with a contact angle of 162° compared with that on a pure copper surface. The results indicated that compared with the pure copper surface, the superhydrophobic modified surface delayed the freezing time by approximately 55 min. Moreover, the ice layer of the superhydrophobic modified surface was loose and light, exhibiting a daisy-like pattern. Kim and Lee [17] conducted defrosting experiments on superhydrophilic, pure copper, and superhydrophobic fin surfaces. They also observed a frosting delay phenomenon on the superhydrophobic fins. Furthermore, the finding revealed that the surface contact angle had no significant effect on the defrosting time.

According to the existing literatures, a patterned wettability area can effectively improve the benefits of condensate drainage; however, this method has rarely been applied to frosting studies. Therefore, the objective of this study is to provide a novel, thorn-shaped, containing, hydrophilic, and hydrophobic surface to have a better condensate drainage characteristic, and it will be shown subsequently that that surface can also delay the required frosting time. The design is made available through screen printing and uses the difference in wettability gradient for achieving surface characteristics such as rapid surface drainage of condensate and frost resistance. Image visualization technology was used to understand its mechanism in depth as the basis for optimal pattern design.

2. Experimental Setup

2.1. Experimental Framework

The diagram of the experimental system used in this study is displayed in Figure 1. The system consisted of an environmental chamber, a frost and defrost water circulation system, a data acquisition system, and a high-speed image system. The system was equipped with two thermostatic baths, namely the thermostatic baths for frosting (EYELA CCA-1111) and defrosting (YSC RC-10), which can offer controlled temperature ranges of -20 to 30 °C and -10 to 100 °C, respectively. Both thermostatic baths were supplied with ethylene glycol solution (60% wt), which can control the inlet water temperature and circulating water volume of the hydrocooling plate for allowing a stable condensate flow with a minimum control temperature of -20 °C. The water circulation system controlled the frost or defrost circuit through a manual three-way valve. A flow regulating valve and flow meter (YOKOGAWA-AXF002G) were installed at the tube inlet for adjustment and monitoring the flow.

After passing through the condensation testing section of the test segment, the flow circulated back to the thermostatic bath and completed the condensate circuit. The flow meter had a measurement range of 0.1–8.0 m³/h and an accuracy of 0.35%. The cold plate of the experiment was placed in the environmental chamber (JOBHO CD-321). The four corners of the front side of the cold plate were fixed by screws so that samples could be easily replaced. The other exposed parts of the cold plate were insulated with polyethylene heat insulating material, and a camera was added in front of the sample to observe and record the surface phenomenon. To confirm the wind speed in the environmental chamber, a unidirectional hot-wire anemometer (Testo 480) was used to measure the airflow velocity from sampling of 20-points. The measuring points of the hot-wire anemometer are located at a virtual plane which is 50 mm apart from the sample. The vertical and horizontal spacing of measuring points are 50 mm and 60 mm, respectively. The hot-wire anemometer had a measurement range of 0 to 20 m/s and an accuracy of $\pm(0.03 \text{ m/s} + 5\%)$. The average airflow velocity was 0.85 m/s.

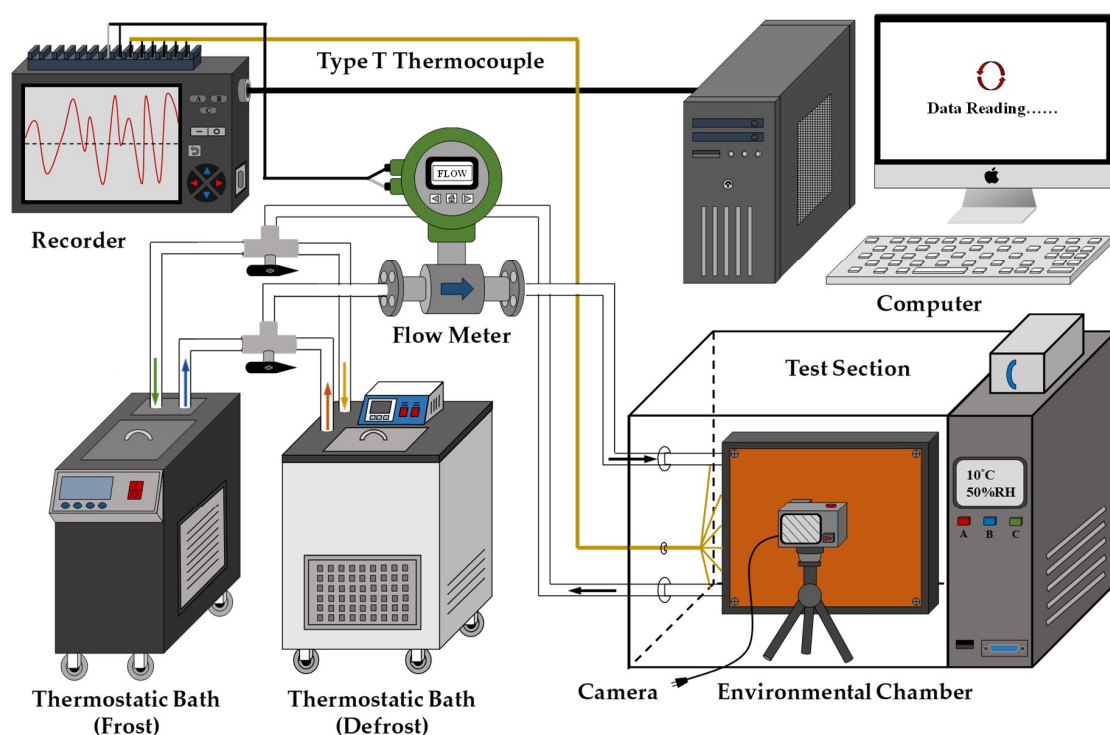


Figure 1. Diagram of the experimental system.

To more accurately evaluate the condensing or frosting performance, nine T-type thermocouples were installed on the back of the test plate sample (Figure 2) for measuring the temperatures at different locations on the bottom surface of the plate. In addition, a heat conduction calculation formula was used to evaluate the differences between the surface and bottom temperatures in the experiment ($<0.01 \text{ }^\circ\text{C}$). Thus, the heat transfer coefficient was directly calculated using the average temperature. The temperature was measured by the T-type thermocouple wires at the frost and defrost water cycle inlet and outlet, and the temperature signals were recorded separately. The temperature variations of the thermocouples were within $0.2 \text{ }^\circ\text{C}$ during the isothermal test. The thermocouples were calibrated using a quartz thermometer with an accuracy of $0.01 \text{ }^\circ\text{C}$ prior to testing for achieving a thermocouple accuracy of $0.1 \text{ }^\circ\text{C}$. All the relevant information was converted by the data acquisition system (GRAPHTEC-GL840) and transmitted to the computer for processing and recording through a web interface. To capture the changes in the patterned surface condensation, frosting, and defrosting, an image system was set up to determine the relative relationship between the flow field change and the heat transfer performance. The camera used in this system was UPMOST-UPG650, which features a shooting speed of more than 30 fps. The camera was placed on a tripod to capture the

pictures of condensation, frosting, and defrosting phase changes on the plate under any operating conditions. Uncertainties in the reported experimental values were estimated by the method suggested by Moffat [18]. The highest uncertainties are 5.83% for the heat transfer coefficient.

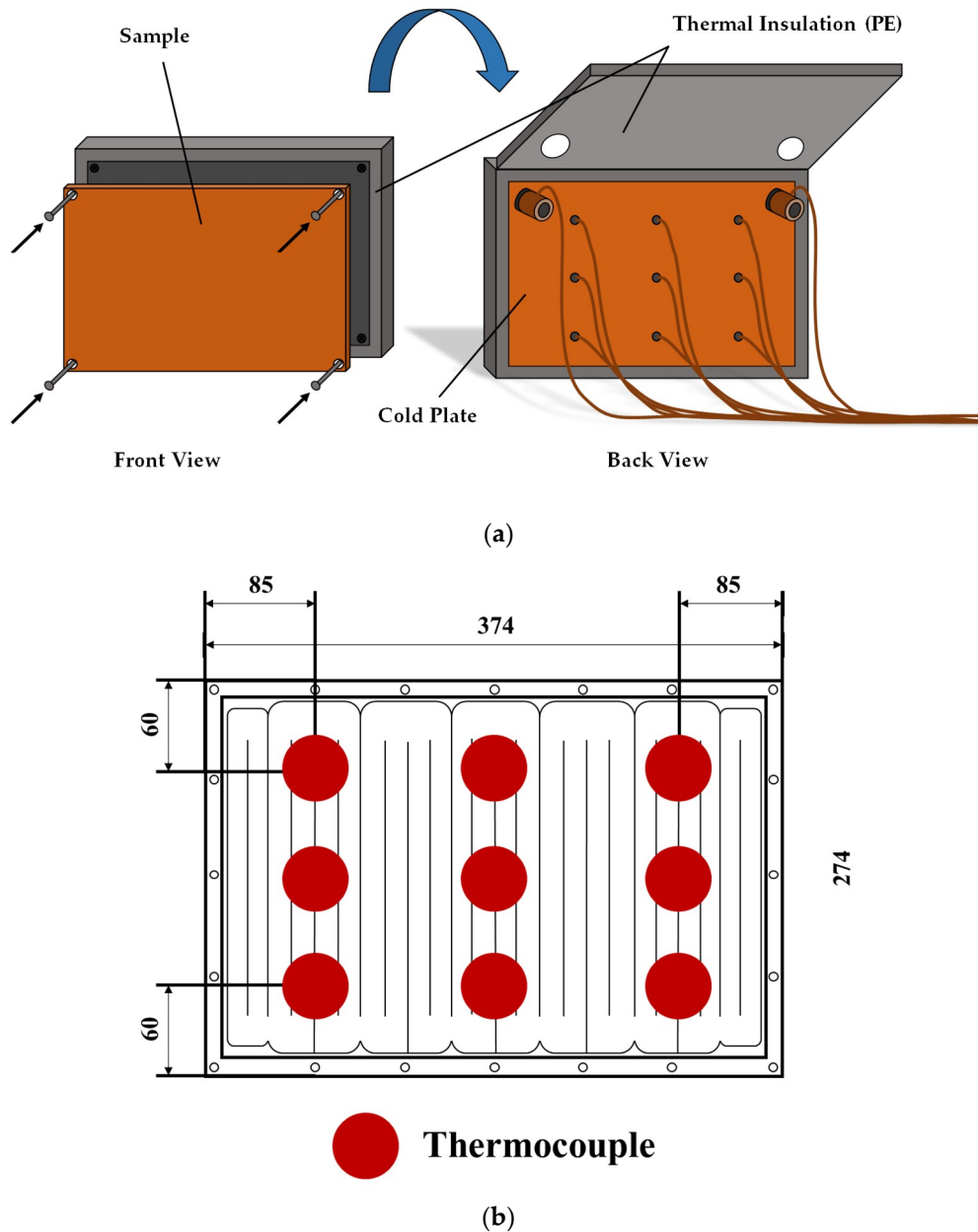


Figure 2. Diagrams of the (a) experimental cold plate and (b) thermocouple setup (unit: mm).

2.2. Parameter Measurement and Discussion

The distance between the front and back surfaces of the copper plate was 5 mm. The temperature difference between both surfaces of the copper plate can be calculated through (1) and (2). The results indicated that the temperature difference between both sides was only within 0.01 °C. Thus, the measured back surface temperature was assumed to be the front surface temperature.

$$Q = k \times A \times \frac{\Delta T}{\Delta x} \quad (1)$$

(ΔT : temperature difference between the front and back surfaces of the copper plate)

$$\Delta T = \frac{Q \times \Delta x}{k \times A} = \frac{40 \times 0.005}{387 \times 0.0875} = 0.0062, \quad (2)$$

The temperature difference ($T_{out} - T_{in}$) between the inlet and outlet of the ethylene glycol solution of the thermostatic bath was calculated to obtain the total heat absorbed by the cold plate. The heat convection coefficient on the air side (h) was estimated from the ambient temperature (T_{air}) and plate temperature (T_s) according to the following formula:

$$Q = \dot{m} \times C_p \times (T_{out} - T_{in}) = h \times A \times (T_{air} - T_s) \quad (3)$$

$$h = \frac{\dot{m} \times C_p \times (T_{out} - T_{in})}{A \times (T_{air} - T_s)} \quad (4)$$

2.3. Patterned Modified Surface

The geometric size of the two samples tested in this study (Figure 3) was $350 \times 250 \times 3 \text{ mm}^3$ (length \times width \times thickness). The two samples, namely a pure copper surface (as a control group) and patterned modified surface, were made of red copper with a heat conductivity of $387 \text{ W/m}\cdot\text{K}$. Red copper has a hydrophilic surface. First, waterproof sandpaper was used to remove the oxide film on the surface, which was polished with a bench grinder. Finally, the surface of the copper plate was cleaned with industrial alcohol and a clean cloth with a contact angle of 65° . The polished red copper sample was set at rest. Then, Teflon paint was poured into a pre-designed thorn-shaped pattern stencil (the molding contact angle was 89°) for printing on the plate surface through manual pushing. The samples were then baked at 150°C for 30 min, and the thorns were obtained after cooling.

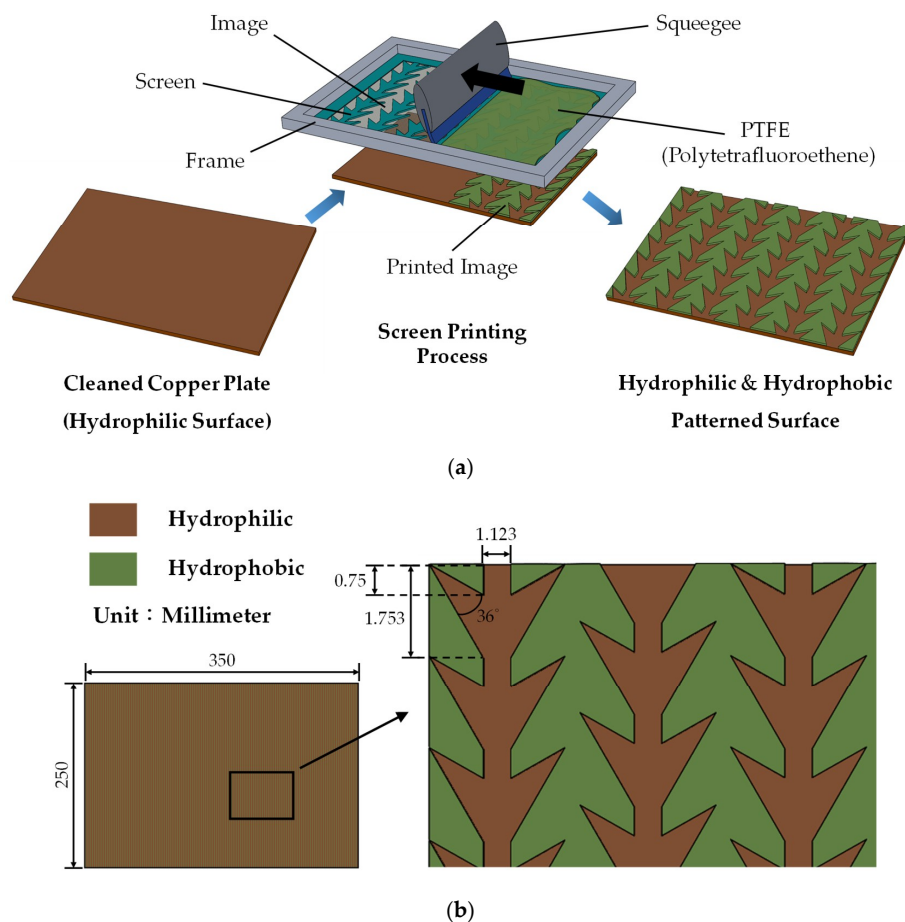


Figure 3. (a) Production process for the mixed patterned surface and (b) thorn dimensions.

2.4. Experimental Principle

The goal of the experiment was to enhance the movement mechanism of the condensate by using different surface structures and pattern changes. According to the relevant literature, differences in the free energy of different wetted surfaces can cause small droplets to move from a less hydrophilic surface to a more hydrophilic surface. When the droplets were at the tip of the hydrophilic area, their force directions diverged. Moreover, the wedge-shaped angle opening of the droplets was set downward to allow the condensate in the Teflon area to move to the polished red copper area for a second time by using gravity to increase its moving force, as depicted in Figure 4a. Finally, the central vertical polished copper drain was designed for the droplets to move to the center. In addition to increasing the combined speed, it can quickly reach the maximum droplet size and slide down while sweeping other droplets on the drain to quickly reduce the surface heat resistance (Figure 5).

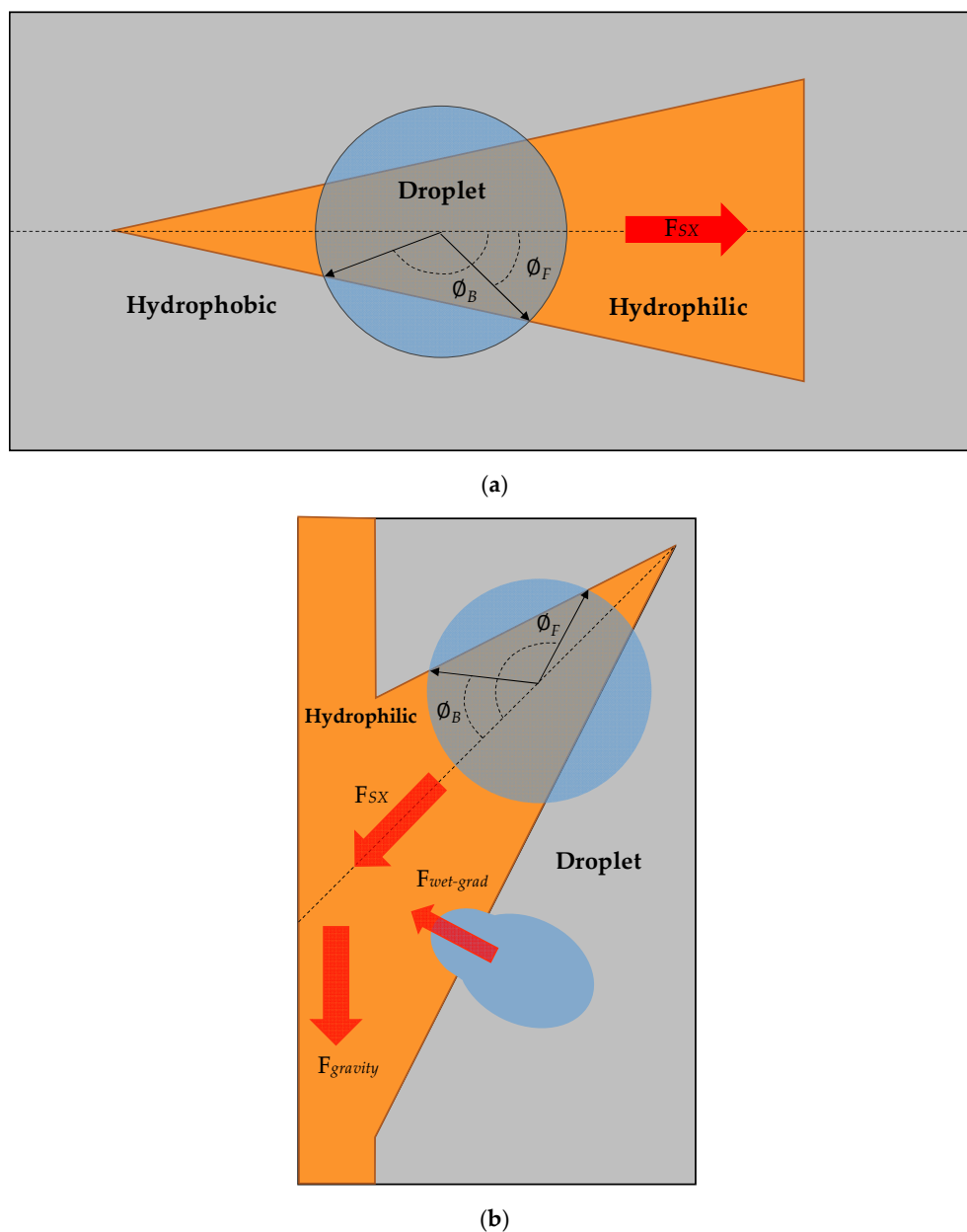


Figure 4. (a) Schematic diagram of the forces acting on the interface (b) Principle of wedge droplet movement.

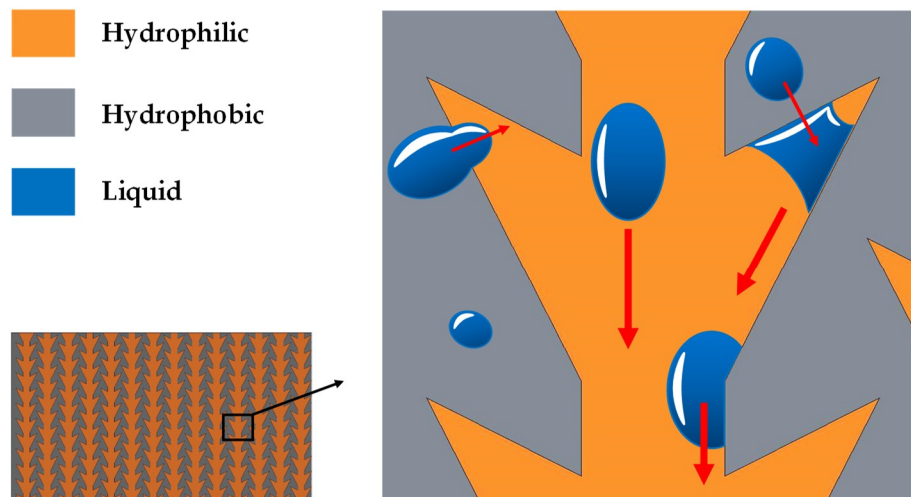


Figure 5. Thorn droplet movement discharging mechanism.

3. Results and Discussion

To evaluate the performance of the patterned modified surface under different designs, condensation, frosting, and defrosting experiments of different surface structure samples were conducted at an ambient temperature of 20 °C, 80% RH, and a flat surface temperature of -8.4 °C. The experimental image of the pure copper surface (Figure 6) reveals a comprehensive condensation and frosting process. First, a condensation phenomenon occurred on the surface of the plate. For elapsed time of 30 min, the droplet accumulated to a threshold size, in which the gravity surpasses the adhesion force. Consequently, slippage began, and a condensation nucleus process occurred. The sliding path mostly comprised vertical strips. Although the aforementioned phenomenon was frequently repeated, a low contact angle of the pure copper surface resulted in high wettability, which caused some of the condensate to remain on the surface after renewal and the formation of irregular filmwise shapes. When time reaches 45 min, the liquid film was completely frozen, and surface renewal could not be performed. Finally, as the ice density strengthened during the ice layer complete growth period, the thickness of the ice layer gradually covered the frozen droplets.

The thorns utilized the differences in free energy between different hydrophilic surfaces, the low wettability of the Teflon pattern, and the high wettability of pure copper surface. When the droplets in the Teflon pattern area touched the junction, parallel adsorption was observed onto the polished copper area, as displayed in Figure 7a. The droplet adsorption and combined force at the Teflon area exhibited an up-moving phenomenon that overcame the influence of gravity (Figure 7b). Because the hydrophilic wedge angle was inclined downwards, the gravity force assisted the droplet in moving, which enhanced the gathering effect of the droplets on the central drainage channel, as illustrated in Figure 7c. When the droplets gradually merged at the central hydrophilic point to yield the maximum droplet size, the surface adhesion was then overpowered by gravity, which caused the droplet to slide down and simultaneously sweep away other droplets on the slip path, as displayed in Figure 8a. A special phenomenon of crossflow passage may occur when the sliding movement changes direction due to droplets on the non-conventional drainage channel, which increases the droplet merger rate as well as the sweeping area during sliding. Moreover, tiny droplets remained in the central drainage channel on the renewed surface mostly, whereas nearly no droplets adhered to the Teflon pattern area. Finally, the condensation process was repeated on the renewed surface, and the changes in size of the droplets are depicted in Figure 9.

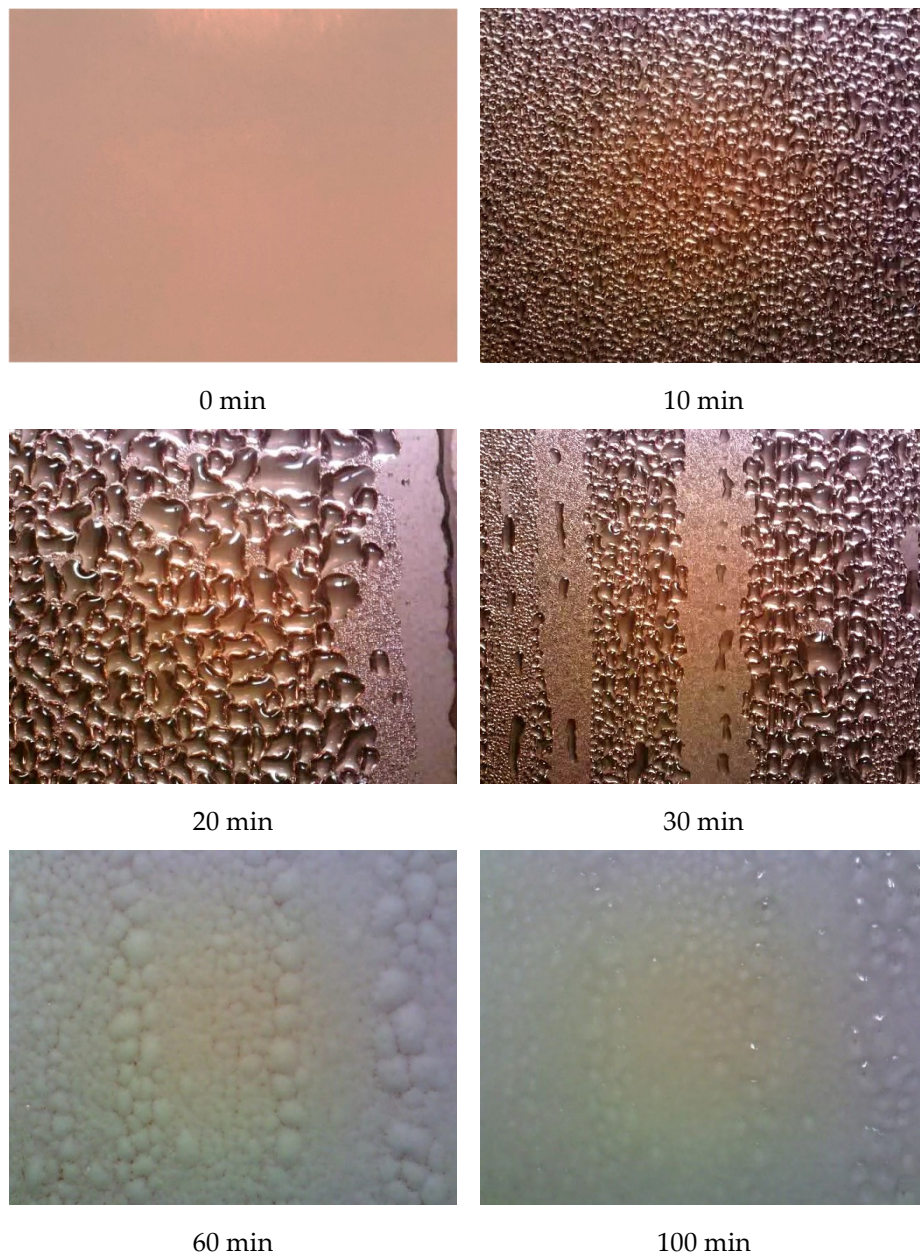


Figure 6. Frosting images of the polished red copper sample (20 °C).

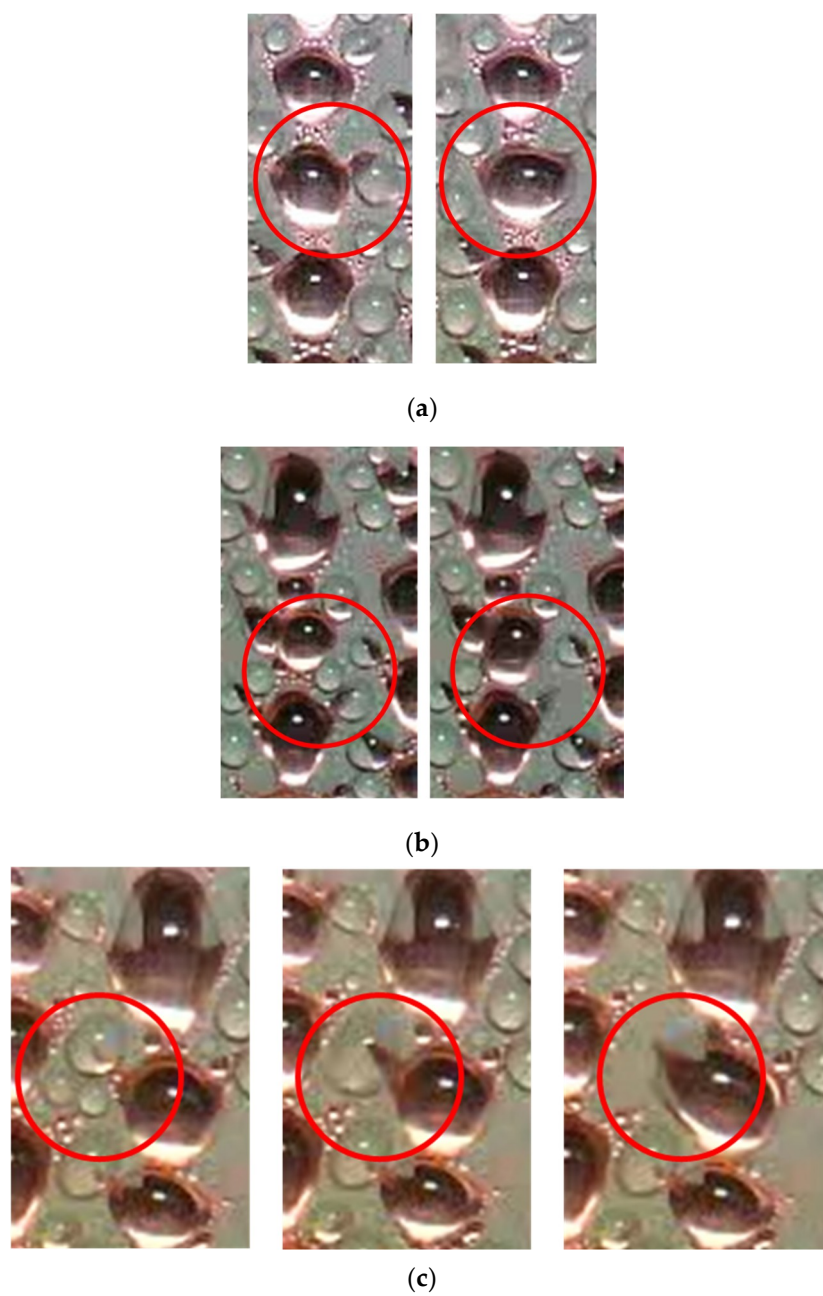
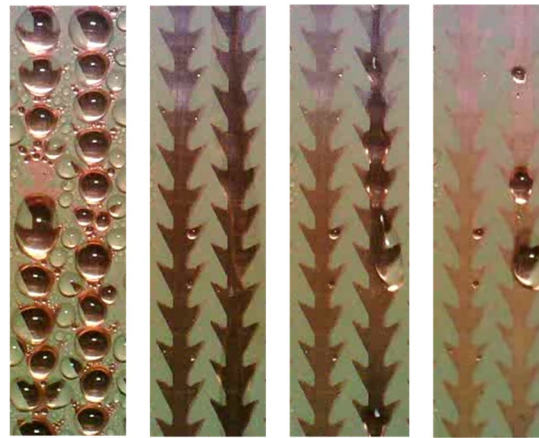


Figure 7. (a) Droplet adsorption phenomenon on the thorn sample; (b) droplet combination and adsorption phenomenon on the thorn sample at 0.5 s; and (c) droplet combination and adsorption phenomenon on the thorn sample at 3 s.



(a)



(b)

Figure 8. (a) Droplet sliding drainage mechanism of the thorn sample and (b) surface renewal cross-flow phenomenon.

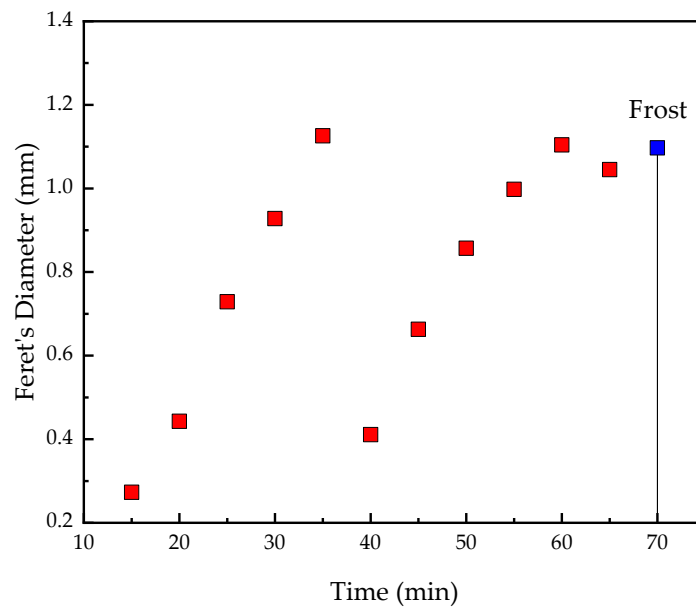


Figure 9. Changes in the thorn sample droplet size.

Due to the surface tension of the thorns, the plate exhibited a frequent surface renewal phenomenon. When the condensed water slid down to the initial frost zone, the slipping phenomenon had the same renewal effect on the thin ice layer on the surface. The sliding condensate destroyed the initially grown ice crystals or the fragile ice layer, which forced the surface to refreeze and consequently resulted in an incomplete surface frosting phenomenon (Figure 10). When the ice layer was thick with a high distribution density, the slid droplets moved and spread across the porous media between the frozen droplets by capillary force, which enlarged the width of the sliding path and increased the renewed frost surface area. This phenomenon can delay the freezing time of the droplets, reduce the thickness of the ice layer and heat resistance, and improve the heat transfer coefficient, as illustrated in Figures 11–13.

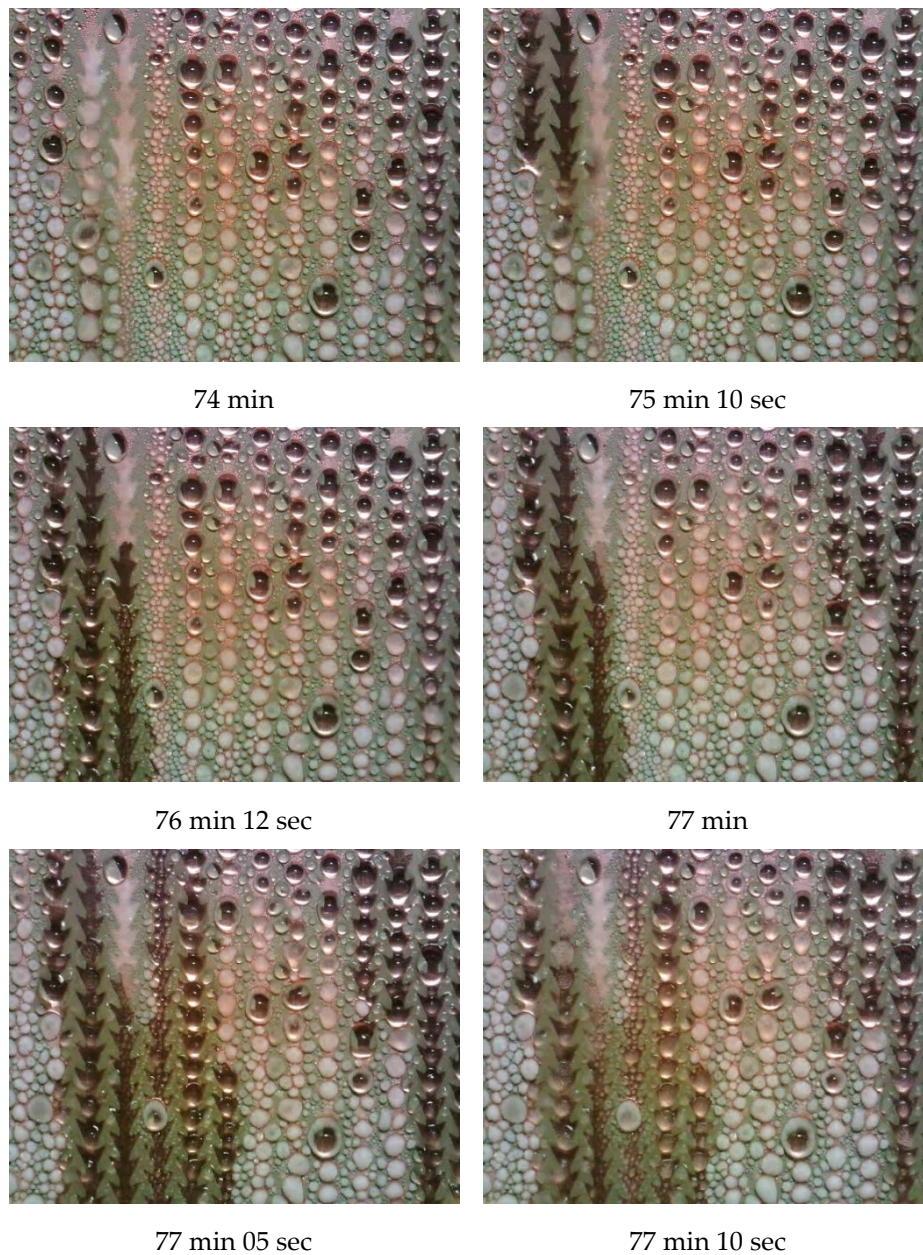


Figure 10. Surface renewal. Images of the frozen surface of the thorn sample.

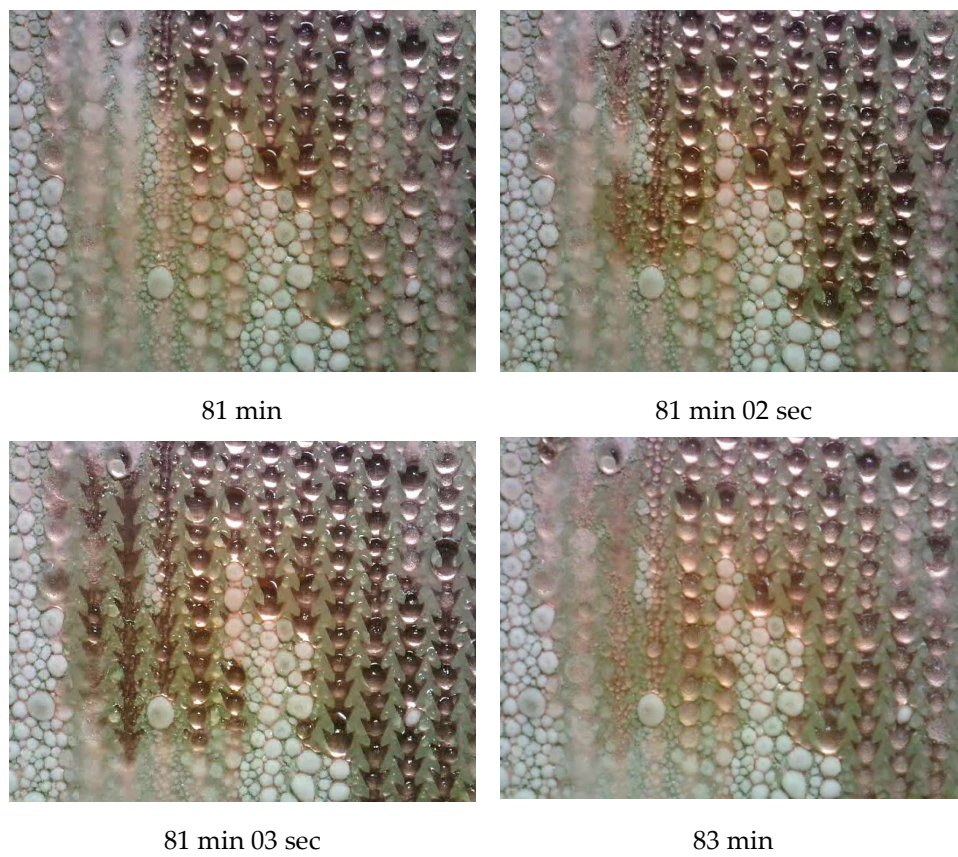


Figure 11. Surface renewal images of the expansion of the frozen surface of the thorn sample.



Figure 12. Porous structure of the ice layer of the thorn sample.

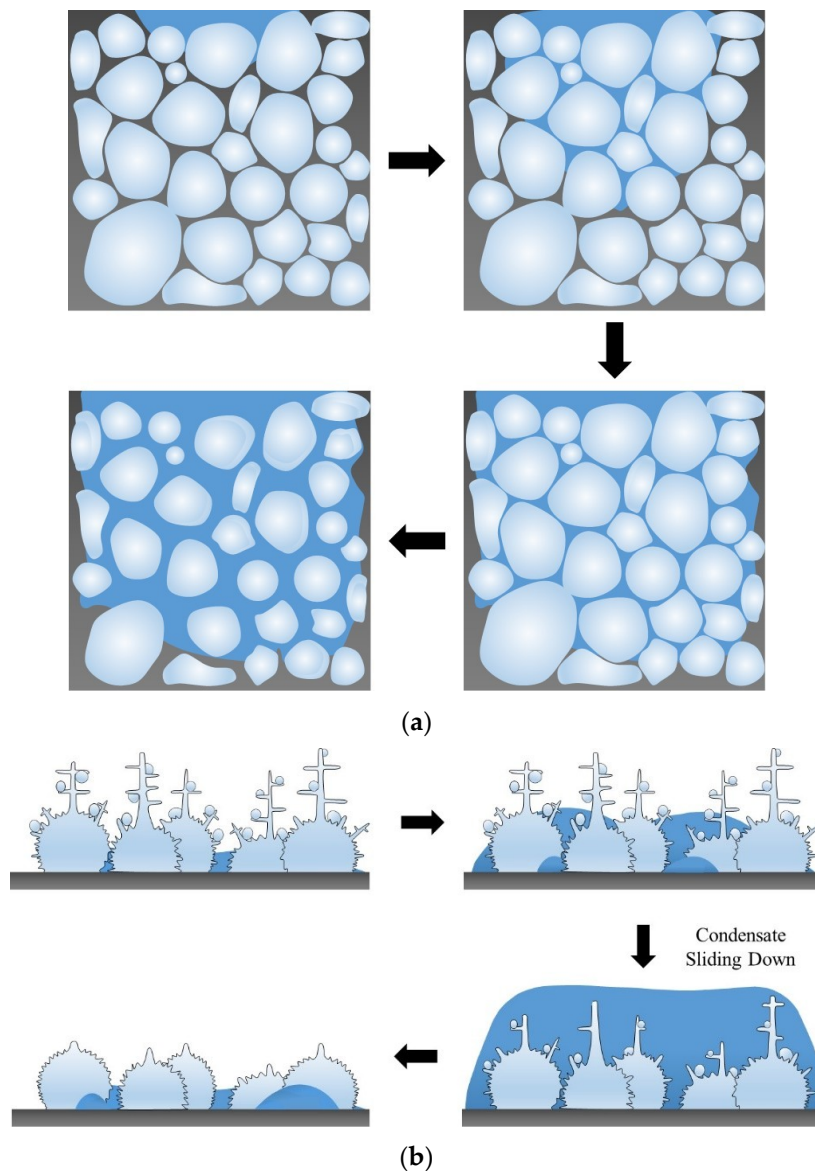


Figure 13. (a) Upper view of condensate surface renewal and (b) side view of condensate surface renewal.

As displayed in Figure 14, the renewal rate of pure copper surface was lower than that of the thorns; however, the surface renewal phenomenon occurred quicker for polished red copper. Therefore, at the time 45 min, the red copper surface condensate had completely frozen, whereas the surface droplets of thorns began to freeze at 75 min and were completely frozen at 90 min. Finally, the ice layer produced after 2 h of frosting was poured in a 30 °C ethylene glycol solution for defrosting and the melting phenomenon was recorded. As displayed in the image, because the polished copper surface had a low contact angle and high wettability, some condensate remained on the surface and exhibited an irregular filmwise state after defrosting. The surface of the thorns had a high surface contact angle and low wettability. Therefore, a strong repulsive force existed between the surface and the melted water. When the thermal solution passed through the internal flow channel, the ice layer in contact with the plate surface as well as the ice surface exposed to the environment melted simultaneously. However, the heat conduction rate decreased because the ice layer was thicker at the middle. Moreover, the melted water in contact with the flat plate was removed, which caused the entire ice layer to be displaced downward. Finally, although the surface of the thorns was relatively clean after defrosting, a small amount of residual water was attached to the center of the red copper drainage channel due to the gravitational effect, which indicated that some hydrophobicity remained in the Teflon pattern area.

during and after the defrost process. However, some large droplets were stuck between the red copper and Teflon pattern areas because the difference in the surface free energy gradient between the two areas formed an active force opposite to that of the gravitational force, which led to excessive contact angle hysteresis, as illustrated in Figure 15.

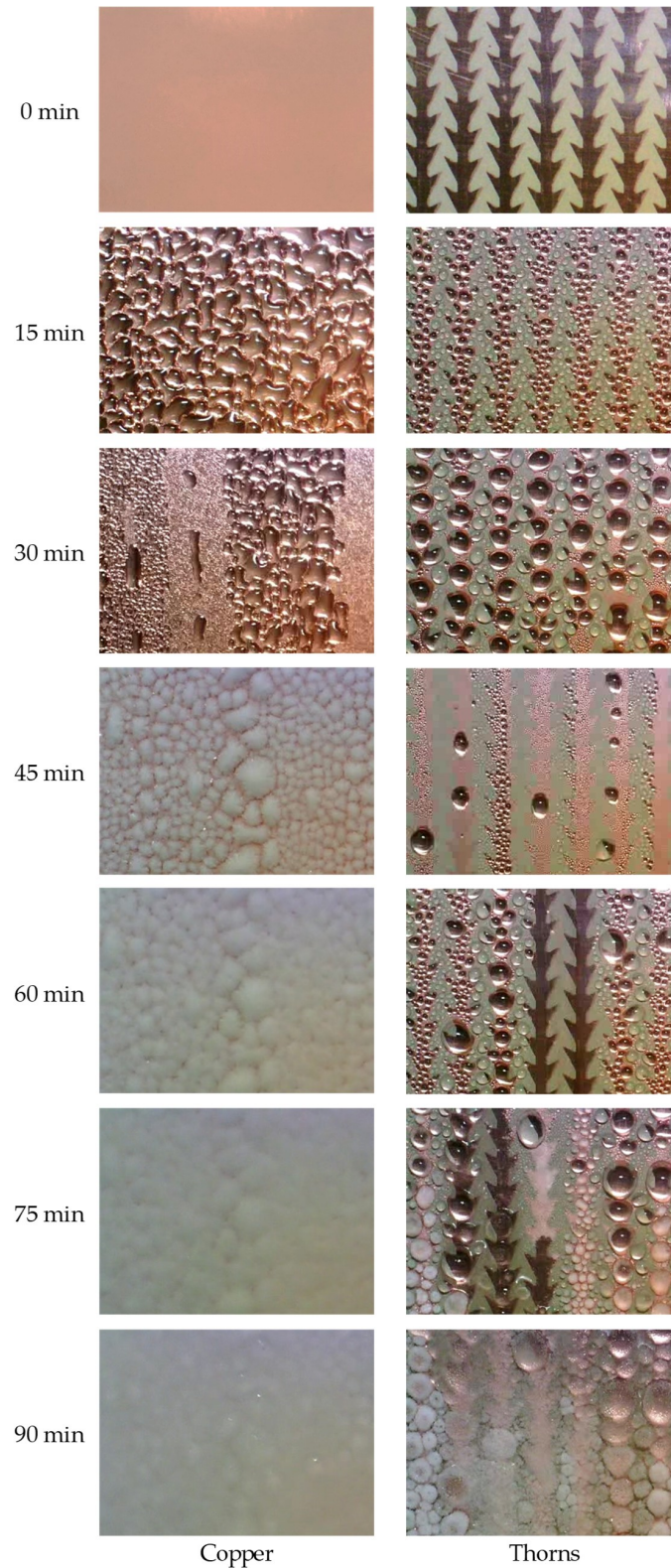


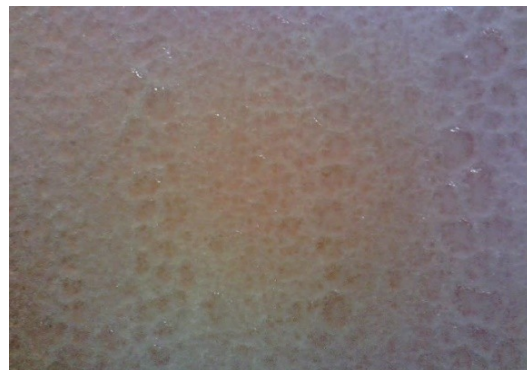
Figure 14. Frosting process of the polished red copper and thorn samples.



0 min



0 min



2 min



2 min



3 min 30 sec



3 min 30 sec



4 min



4 min

Figure 15. Defrosting process of the polished red copper and thorn samples.

According to the abovementioned observations, three parameters are discussed, namely the heat transfer coefficient during the frosting period, time required for the ice layer to completely cover the surface, and time required for defrosting. Because the surface of the thorns exhibited an incompletely frozen state during the frosting period and steady and frequent condensate renewal occurred continuously, a high surface heat exchange efficiency was achieved (Figure 16). Therefore, the heat transfer coefficient of the thorns was approximately 16.2% higher than that of the polished red copper sample. Furthermore, the time required for the complete growth of the ice layer was approximately 52.4% higher for the thorns than for polished red copper. Nonetheless, both samples had nearly identical defrosting time efficiencies.

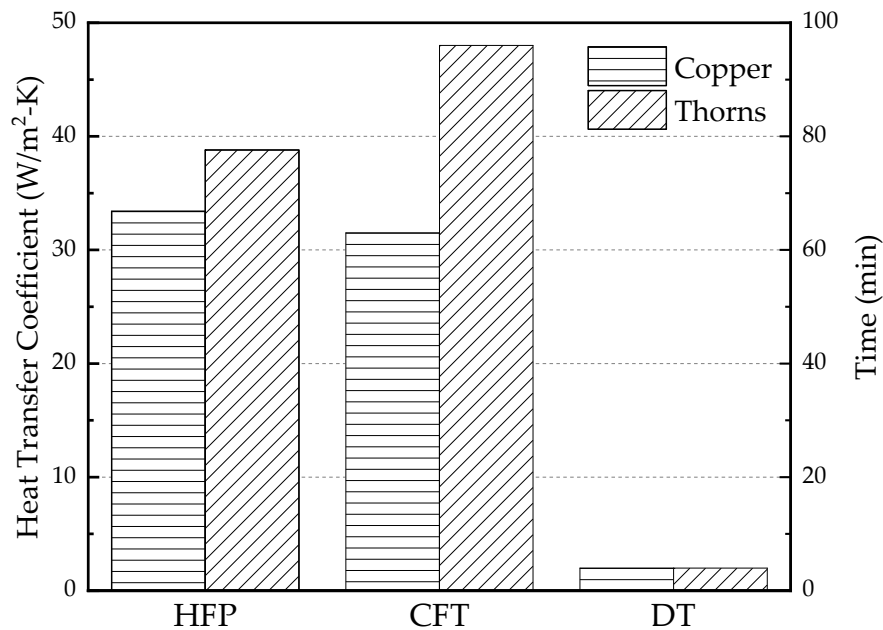


Figure 16. Comparison chart for the polished red copper and thorn samples. HFP–Heat transfer coefficient during frosting period. CFT– Complete frosting time. DT– Defrost time.

4. Conclusions

In this study, a cold plate with a patterned hydrophobic and hydrophilic mixed surface was used. In addition, a patterned thorn sample was developed with reference to the results of the relevant literatures. Different types of coatings and chemical treatments were designed for the pattern so that it exhibited the condensate drainage effect on the surface without relying on external force and could control the temperature of the inlet solution to cause condensation and frosting on the surface of the sample. Moreover, a camera set in front of the sample was used to simultaneously record the surface images. Finally, the results for the patterned thorn sample were compared with those for the polished red copper sample, and the following conclusions were obtained:

- (1) Surface renewal was observed in the condensed part of the polished red copper sample. Moreover, the central drainage effect of droplet adsorption and combination on the patterned thorn samples was significant and occurred frequently.
- (2) The thorns exhibited the mechanisms of droplet movement, combination, and central drainage, which increased the surface renewal rate and inhibited ice layer growth by 52.4% when compared with that for polished red copper. In addition, the heat transfer coefficient of the thorn sample increased by approximately 16.2% compared with that of polished red copper during the frosting period.
- (3) Although both samples had almost similar defrosting times, the residual water after defrosting did not form an irregular liquid film on the thorn sample, which had only a limited amount of

adhered water, because it had a lower overall wettability and higher repulsive force on the melted water compared with the polished red copper sample. However, some of the large droplets were likely to stagnate at the structural junction due to contact angle hysteresis.

Author Contributions: All the authors have contributed their efforts to complete the paper. K.-S.Y. supervised the work and review and editing of the manuscript. W.L. conducted the experiments and wrote the first draft, Y.-L.W. provided supervised the experiment and technical assistance.

Funding: The authors are indebted to the financial support from the Ministry of Science and Technology, Taiwan under contract MOST 108-3116-F-167 -001 -CC1.

Conflicts of Interest: The authors declare no conflict of interest.

Nomenclature

A	surface area, (m ²)
C_p	heat capacity, (J/kg-K)
F	surface force, (N/m)
h	heat transfer coefficient, (W/m ² -K)
k	thermal conductivity, (W/m – K)
\dot{m}	mass flow rate, (kg/s)
Q	heat transfer rate, (W)
T	temperature, (K)
ϕ	azimuthal angle of droplet, (°)

Subscripts

<i>air</i>	ambient air
<i>B</i>	back of the droplet
<i>F</i>	front of the droplet
<i>gravity</i>	gravity
<i>in</i>	inlet
<i>out</i>	outlet
<i>S</i>	surface
<i>X</i>	x-direction
<i>wet-grad</i>	gradient of wettability

References

- Emery, A.F.; Siegel, B.L. Experimental measurements of the effects of frost formation on heat exchanger performance. In Proceedings of the AIAA/ASME Thermophysics and Heat Transfer Conference, Seattle, WA, USA, 18–20 June 1990; pp. 1–8.
- Amer, M.; Wang, C.-C. Review of defrosting methods. *Renew. Sustain. Energy Rev.* **2017**, *73*, 53–74. [[CrossRef](#)]
- Joppolo, C.M.; Molinaroli, L.; De Antonellis, S.; Merlo, U. Experimental analysis of frost formation with the presence of an electric field on fin and tube evaporator. *Int. J. Refrig.* **2012**, *35*, 468–474. [[CrossRef](#)]
- Liu, Z.; Wang, H.; Zhang, X.; Meng, S.; Ma, C. An experimental study on minimizing frost deposition on a cold surface under natural convection conditions by use of a novel anti-frosting paint. Part I. Anti-frosting performance and comparison with the uncoated metallic surface. *Int. J. Refrig.* **2006**, *29*, 229–236. [[CrossRef](#)]
- Young, T. An Essay on the Cohesion of Fluids. *Philos. Trans. R. Soc. Lond.* **1805**, *95*, 65–87. [[CrossRef](#)]
- Vemuri, S.; Kim, K.J. An experimental and theoretical study on the concept of dropwise condensation. *Int. J. Heat Mass Transf.* **2006**, *49*, 649–657. [[CrossRef](#)]
- Ma, X.-H.; Zhou, X.-D.; Lan, Z.; Li, Y.-M.; Zhang, Y. Condensation heat transfer enhancement in the presence of non-condensable gas using the interfacial effect of dropwise condensation. *Int. J. Heat Mass Transf.* **2008**, *51*, 1728–1737. [[CrossRef](#)]
- Chatterjee, A.; Derby, M.M.; Peles, Y.; Jensen, M.K. Enhancement of condensation heat transfer with patterned surfaces. *Int. J. Heat Mass Transf.* **2014**, *71*, 675–681. [[CrossRef](#)]

9. Peng, B.; Ma, X.; Lan, Z.; Xu, W.; Wen, R. Experimental investigation on steam condensation heat transfer enhancement with vertically patterned hydrophobic–hydrophilic hybrid surfaces. *Int. J. Heat Mass Transf.* **2015**, *83*, 27–38. [[CrossRef](#)]
10. Alwazzan, M.; Egab, K.; Peng, B.; Khan, J.; Li, C. Condensation on hybrid-patterned copper tubes (I): Characterization of condensation heat transfer. *Int. J. Heat Mass Transf.* **2017**, *112*, 991–1004. [[CrossRef](#)]
11. Alwazzan, M.; Egab, K.; Peng, B.; Khan, J.; Li, C. Condensation on hybrid-patterned copper tubes (II): Visualization study of droplet dynamics. *Int. J. Heat Mass Transf.* **2017**, *112*, 950–958. [[CrossRef](#)]
12. Yang, K.-S.; Lin, K.-H.; Tu, C.-W.; He, Y.-Z.; Wang, C.-C. Experimental investigation of moist air condensation on hydrophilic, hydrophobic, superhydrophilic, and hybrid hydrophobic-hydrophilic surfaces. *Int. J. Heat Mass Transf.* **2017**, *115*, 1032–1041. [[CrossRef](#)]
13. Yang, K.S.; Huang, Y.-Y.; Liu, Y.-H.; Wu, S.-K.; Wang, C.-C. Enhanced dehumidification via hybrid hydrophilic/hydrophobic morphology having wedge gradient and drainage channels. *Heat Mass Transf.* **2019**, *55*, 3359–3368. [[CrossRef](#)]
14. Alheshibri, M.H.; Rogers, N.G.; Sommers, A.D.; Eid, K.F. Spontaneous movement of water droplets on patterned Cu and Al surfaces with wedge-shaped gradients. *Appl. Phys. Lett.* **2013**, *102*, 174103. [[CrossRef](#)]
15. Mahapatra, P.S.; Ghosh, A.; Ganguly, R.; Megaridis, C.M. Key design and operating parameters for enhancing dropwise condensation through wettability patterning. *Int. J. Heat Mass Transf.* **2016**, *92*, 877–883. [[CrossRef](#)]
16. Liu, Z.; Gou, Y.; Wang, J.; Cheng, S. Frost formation on a super-hydrophobic surface under natural convection conditions. *Int. J. Heat Mass Transf.* **2008**, *51*, 5975–5982. [[CrossRef](#)]
17. Kim, K.; Lee, K.-S. Frosting and defrosting characteristics of a fin according to surface contact angle. *Int. J. Heat Mass Transf.* **2011**, *54*, 2758–2764. [[CrossRef](#)]
18. Moffat, R.J. Describing the uncertainties in experimental results. *Exp. Therm. Fluid Sci.* **1988**, *1*, 3–17. [[CrossRef](#)]



© 2019 by the authors. Licensee MDPI, Basel, Switzerland. This article is an open access article distributed under the terms and conditions of the Creative Commons Attribution (CC BY) license (<http://creativecommons.org/licenses/by/4.0/>).